Part I

Advanced white light interferometry

Chapter 2 High-speed white light interferometry

2.1 Research background and goal

As mentioned in Chapter 1, the measurement object of the phase shifting interferometry is limited to the smooth surface, so the white light interferometry is predominantly used in the industrial world. For example, if a bump of a semiconductor IC is to be measured, the bump height is several tens of μm, so phase shifting interferometry cannot be used.

Although many algorithms have been proposed for white light interferometry, the following are typical algorithms from a practical point of view.

(1) Low-pass filter method: The AC component of intensity is squared, the envelope is obtained by the low-pass filter, and the peak position is detected [Caber 1993].

(2) Hilbert transform method: Obtain a waveform with a 90° phase shift, find the envelope, and detect the peak position [Chim et al. 1992].

(3) Centroid method: Squares the AC component of intensity and finds the centroid position of the obtained waveform [Dändliker et al. 1992].

(4) Frequency domain method (FDA method): Fourier transform of the interference waveform is performed to obtain the slope ($d\phi/dk$) of the phase ϕ with respect to the wave number k near the peak of the amplitude spectrum. Since the phase ϕ, height h, and wave number k have a relationship of $\phi = kh$, the height h can be obtained from $h = d\phi/dk$ [de Groot et al. 1993; de Groot et al. 1995].

In either method, the sampling interval needs to be sufficiently narrow and the measurement speed is slow. In order to solve this problem, we propose a speed-up algorithm that uses the technique of waveform reconstruction.

2.2 New algorithm —SEST method—

Consider reconstructing the original waveform from the sampled values of the interference waveform shown in Fig. 1-8. According to Sometani-Shannon's sampling theorem (low-pass sampling theorem), the sampling interval must be less than the Nyquist interval for complete reconstruction. However, in white light interferometry, the interference waveform is band-limited in response to the band limitation of illumination light. Using this property, the authors have developed a new algorithm [SEST (=*Squared Envelope function estimation by Sampling Theory*) that finds the peak position of the interference waveform sampled at a much wider interval (sub-Nyquist sampling) than the sampling interval that satisfies the Nyquist theorem [Hirabayashi et al 2000, Kitagawa et al 2000, Hirabayashi et al. 2002] [1)]. The outline of the SEST algorithm is described below.

2.2.1 Wavelength band of white-light interference waveform

The frequency band of the interference waveform of white light interferometry is limited by the wavelength band of the light source. This is because the interference intensity of white light interferometry is the sum of the interference intensities of each wavelength and is expressed by the following equation:

[1)] This algorithm differs from the usual sampling theorem in that it restores another function, i.e. the squared envelope function, from the sampled values of the interferogram, which is the original waveform. Therefore, it is also called "generalized sampling theorem".

$$g(z) = C + \int_{\lambda_1}^{\lambda_2} I(\lambda)\cos(4\pi(z - z_0)/\lambda)\, d\lambda\,, \tag{2-1}$$

where g(z) is the intensity at the scanning position z, C is the DC component, z_0 is the height of the measurement target, λ is the wavelength, and λ_1 and λ_2 are the upper and lower limits of the wavelength of the measurement light. In addition, $I(\lambda)$ is the spectrum that combines the illumination light and the imaging system.

The wavelength band of this signal is limited to [λ_1, λ_2]. It is also possible to limit the band to any band by inserting a bandpass filter in the illumination optical path. Figure 2-1 shows the measured interferogram and the frequency spectrum obtained by Fourier transform (the horizontal axis is converted to wavelength) under three illumination conditions:

(1) no filter,

(2) a filter with a bandwidth of 80 nm,

(3) a filter with a bandwidth of 40 nm.

The center wavelength of the filter is 600 nm. The band of the interference signal is limited according to the bandwidth of the inserted filter.

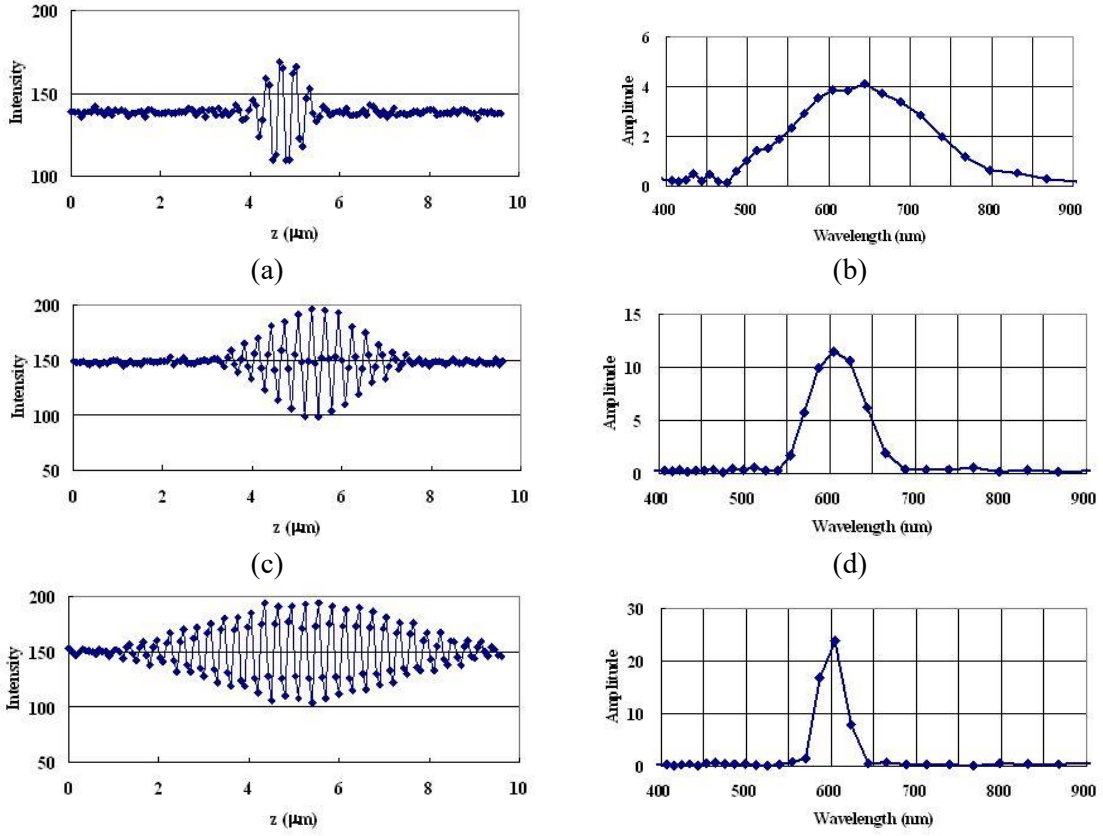

Fig. 2-1 Interferograms and their spectra under three illumination conditions. (a)(b): without filter; (c)(d): with an 80-nm bandwidth filter; (e)(f) with a 40-nm bandwidth filter.

2.2.2 Reconstruction of band-limited signal

Define *f(z)* as the signal excluding the DC component irrelevant to height measurement from

Eq. (2-1), then

$$f(z) = \int_{\lambda_1}^{\lambda_2} I(\lambda) \cos(4\pi(z - z_0)/\lambda)\, d\lambda \,. \tag{2–2}$$

Since the interference waveform is band-limited corresponding to the wavelength band $[\lambda_1, \lambda_2]$ of the illumination light, the band-pass sampling theorem [Kohlenberg 1953] can be applied, and $f(z)$ can be expressed using its sampled data $f(z_n)\,(n = -\infty \sim +\infty)$ as follows:

$$f(z) = \sum_{n=-\infty}^{\infty} f(z_n)\phi_n(z)\,, \tag{2–3}$$

where $\phi_n(z)$ is a function defined below:

$$\phi_n(z) = \mathrm{sinc}\left[\frac{\pi(z - z_n)}{2\Delta}\right] \cos\left[\frac{4\pi(z - z_n)}{\lambda_c}\right]. \tag{2–4}$$

Also, Δ is the sampling interval and requires certain conditions. The details will be described in the next section.

By the way, since there are a finite number of sample values in an actual system, we truncate the infinite series of Eq. (2-3) at the N-th term, and by defining f_j as the AC component obtained by removing the DC component C from the observed value $g(z_j)$, which is expressed as the following equation,

$$f_j = g(z_j) - C\,, \tag{2–5}$$

then we get the reconstructed interference waveform $f_B(z)$ as follows:

$$f_B(z) = \sum_{n=0}^{N-1} f_n \phi_n(z) \,. \tag{2–6}$$

2.2.3 White-light interference signal model and envelope function

Next, let us consider an algorithm that detects the peak position of the interference waveform. As shown in Fig. 2-1, the interference waveform is sinusoidal with a period of almost $\lambda/2$, and if the sampling interval is wide, it is difficult to find the peak position correctly. Therefore, let us consider obtaining the envelope function of the interference waveform. Note that this idea is the same as the Hilbert transform method of the conventional algorithms described in Section 2.1.

By introducing the angular wavenumber defined as $k = 2\pi/\lambda$ to simplify the expression, Eq. (2-1) becomes:

$$f(z) = \int_{k_l}^{k_u} I(k) \cos[2k(z - z_0)]\, dk\,, \tag{2–7}$$

where $[k_l,\ k_u]$ is the band width of the angular wavenumber, and $I(k)$ is the spectrum of the

optics.

Furthermore, defining k_c as the center of the band width, and substituting $k = k_c + (k - k_c)$ into Eq. (2-7),

$$f(z) = m_c(z)\cos[2k_c(z - z_0)] - m_s(z)\sin[2k_c(z - z_0)], \tag{2–8}$$

where

$$m_c(z) = \int_{k_l}^{k_u} I(\lambda)\cos[2(k - k_c)(z - z_0)]\,dk, \tag{2–9}$$

$$m_s(z) = \int_{k_l}^{k_u} I(\lambda)\sin[2(k - k_c)(z - z_0)]\,dk. \tag{2–10}$$

By modification, Eq. (2-8) can be written as

$$f(z) = \sqrt{\{m_c(z)\}^2 + \{m_s(z)\}^2}\cos[2k_c(z - z_0) - \varphi], \tag{2–11}$$

where

$$\varphi = \arctan\{-m_c(z)/m_s(z)\}. \tag{2–12}$$

From Eq. (2-11) we can express the envelope function $m(z)$ as:

$$m(z) = \sqrt{\{m_c(z)\}^2 + \{m_s(z)\}^2}. \tag{2–13}$$

For practical use, this paper uses the following squared envelope function (hereinafter referred to as the envelope function).

$$r(z) = \{m_c(z)\}^2 + \{m_s(z)\}^2. \tag{2–14}$$

2.2.4 Estimation of the envelope function

The envelope function $r(z)$ can be obtained from the reconstructed interference waveform. However, what is finally desired is the peak position of the envelope function, and the interference waveform itself is unnecessary. Therefore, by deriving the equation for directly obtaining the estimated value $r_N(z)$ of the envelope function from the sampled value of the interference waveform, the following equation is obtained.

That is, when the sampling points are $z_j = j\Delta$, the envelope function can be reconstructed by the following equation using only the sampled value f_j ($j = 0,1,\cdots, N–1$).

(1) when z is the sampling point, that is, $z = z_j$ ($j = 0,1,\cdots, N–1$):

$$r_N(z_j) = (f_j)^2 + (4/\pi^2)\left\{\sum_{n=-\lfloor (j+1)/2\rfloor}^{\lfloor (N-j-2)/2\rfloor} \frac{f_{j+2n+1}}{2n+1}\right\}^2. \tag{2–15}$$

(2) when z is not any sampling point:

$$r_N(z) = (2\Delta^2/\pi^2)\left[(1-\cos(\pi z/\Delta))\left\{\sum_{n=0}^{\left\lfloor\frac{N-1}{2}\right\rfloor}\frac{f_{2n}}{z-z_{2n}}\right\}^2 + (1+\cos(\pi z/\Delta))\left\{\sum_{n=0}^{\left\lfloor\frac{N}{2}\right\rfloor-1}\frac{f_{2n+1}}{z-z_{2n+1}}\right\}^2\right]. \quad (2\text{–}16)$$

The maximum point of the envelope function is obtained by calculating $r_N(z_j)$ at the sampling points using Eq. (2-15) and performing an interpolative search for the peak near the maximum value using Eq. (2-16).

The SEST algorithm described above is illustrated in Fig. 2-2. The squared envelope function is directly estimated from the intensity data sampled at sub-Nyquist intervals, and then its peak position is obtained.

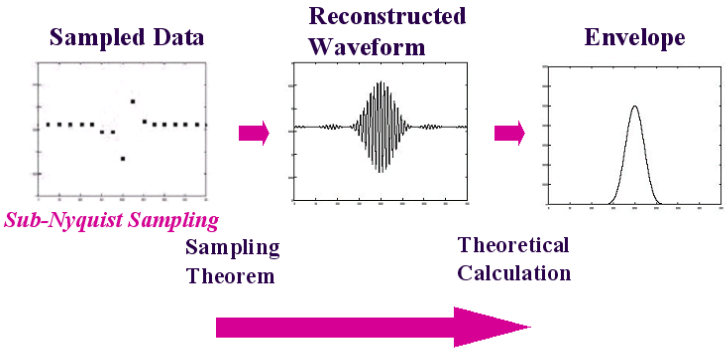

Fig. 2-2 Concept of the SEST algorithm

2.3 Selection of the sampling interval

In order to reconstruct a waveform by the bandpass sampling theorem, the sampling interval Δ must satisfy the following conditions:

$$(I-1)(\lambda_c+\lambda_b)/4 \le \Delta \le I(\lambda_c-\lambda_b)/4, \quad (2\text{–}17)$$

where, λ_c is the center wavelength of the band, λ_b is a half of the band width, I is an integer which satisfies the following condition:

$$1 \le I \le (\lambda_c+\lambda_b)/2\lambda_b. \quad (2\text{–}18)$$

If the condition in Eq. (2-17) is expressed as the non-permissible range $\overline{\Delta}$ of sampling interval, the following equation is obtained.

$$I\frac{\lambda_c-\lambda_b}{4} < \overline{\Delta} < I\frac{\lambda_c+\lambda_b}{4}. \quad (2\text{–}19)$$

The numerators $\lambda_c - \lambda_b$ and $\lambda_c + \lambda_b$ of Eq. (2-19) are the minimum and maximum values of the wavelength band of the interference light respectively, so this formula means that we cannot use a sampling interval that is an integer multiple of 1/2 of the period of the interference waveform.

The maximum allowable sampling interval $\Delta_{\max}$ is given by the following equation from Eqs. (2-17) and (2-18).

$$\Delta_{\max} = \frac{1}{4}\left\lfloor \frac{\lambda_c + \lambda_b}{2\lambda_b} \right\rfloor (\lambda_c - \lambda_b), \tag{2–20}$$

where $\lfloor x \rfloor$ means the maximum integer which does not exceed x.

As an actual example, when λ_c = 600 nm and λ_b = 20 nm, the sampling interval can have 15 ranges as shown in Fig. 2-3. The maximum sampling interval is 2.175 μm, which is 15 times the Nyquist interval.

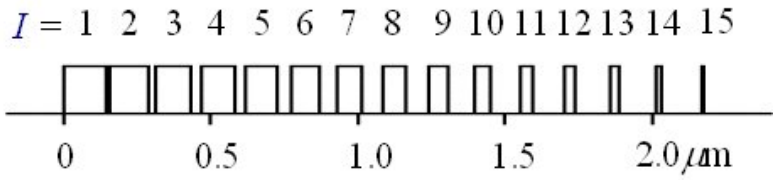

Fig. 2-3 Sampling interval belonging to these 15 blocks can be used for reconstruction of $r(z)$ when the optical filter of λ_c=600nm and λ_b=20nm is used.

2.4 Computer experiments

In order to verify the above algorithm, a computer experiment was conducted using the interference waveform data generated by the theoretical model of Eq. (2-2). As in the previous section, the spectrum of the optical system was λ_c = 600 nm, λ_b = 20 nm, that is, λ_1 = 580 nm, λ_2 = 620 nm, and $I(\lambda)$ = 1 was assumed. Also, the scanning range was set to 0 to 40 μm, and the surface height z_0 = 20μm. The sampling interval Δ was set to 2.175 μm, which is the maximum allowable value.

Figures 2-4 and 2-5 show the generated waveform data $f(z)$, sample point data $f(z_j)$, and waveform $f_B(z)$ reconstructed using the sample values. The plots of $f(z)$ and $f_B(z)$ overlap and shows that the waveform reconstruction is almost complete. Figure 2-6 shows the square root of the envelope function $r_N(z)$ estimated using the sampled data $f(z_j)$. The envelope can be estimated almost correctly, and the peak position is 20μm.

Next, Figs. 2-7 to 2-9 show the results when Gaussian noise (with zero mean and variance σ 0.05) was added to the generated waveform data. The waveform before adding noise is almost reconstructed, and the envelope function is estimated almost correctly.

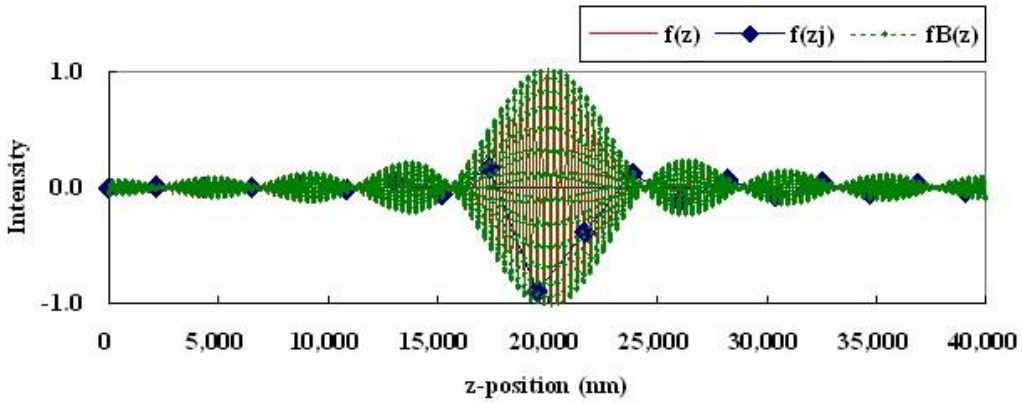

Fig. 2-4 Original interferogram $f(z)$, its sampled data $f(z_j)$ and the reconstructed data $f_B(z)$

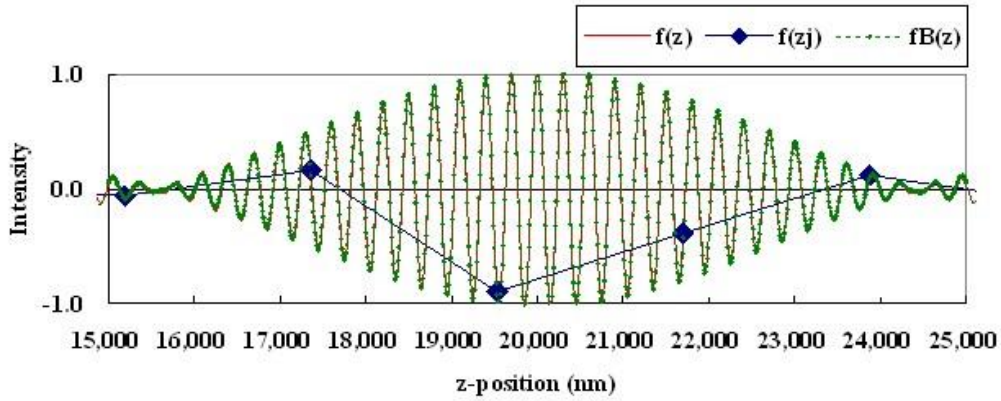

Fig. 2-5 Enlarged graph of Fig. 2-4

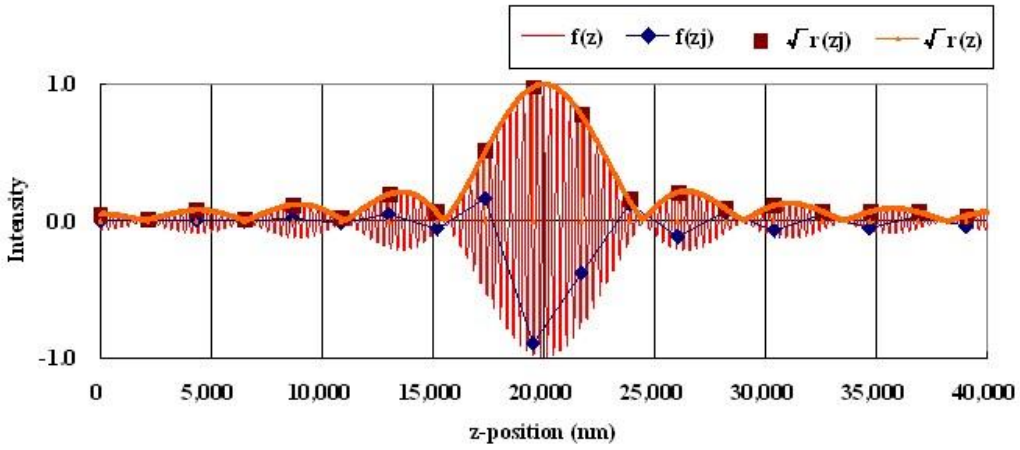

Fig. 2-6 Original interferogram $f(z)$, its sampled data $f(z_j)$ and the reconstructed envelope function $\sqrt{r(z)}$

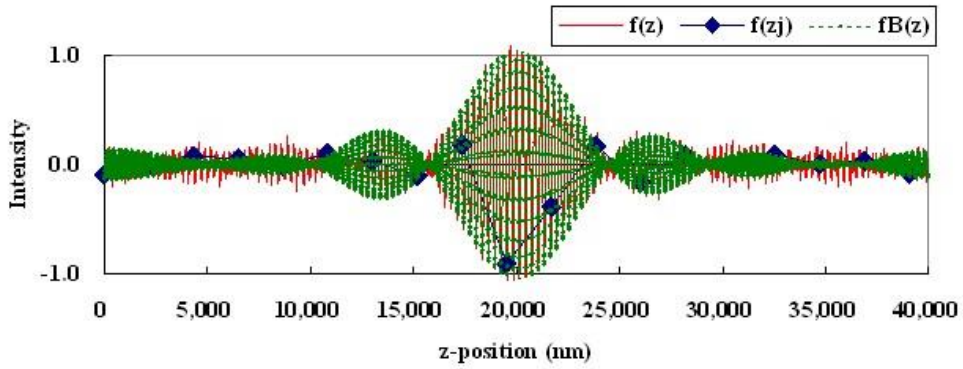

Fig. 2-7 Original interferogram $f(z)$, its sampled data $f(z_j)$ and the reconstructed data $f_B(z)$ (with Gaussian noise added)

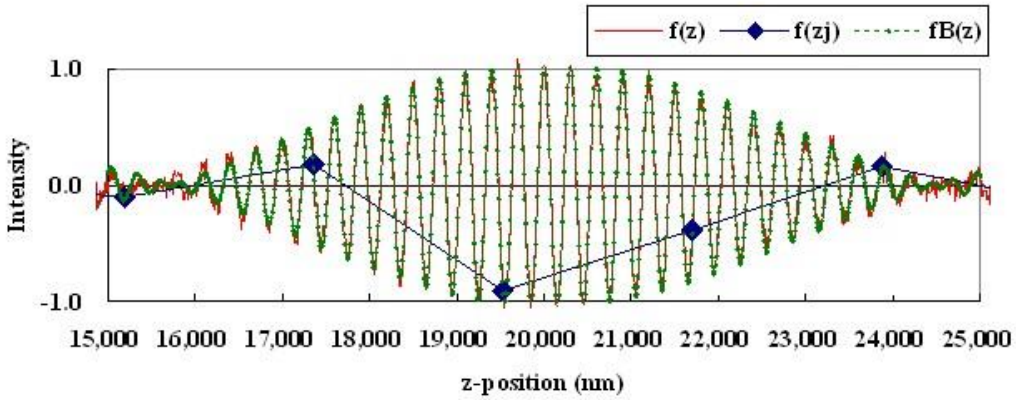

Fig. 2-8 Enlarged graph of Fig. 2-7

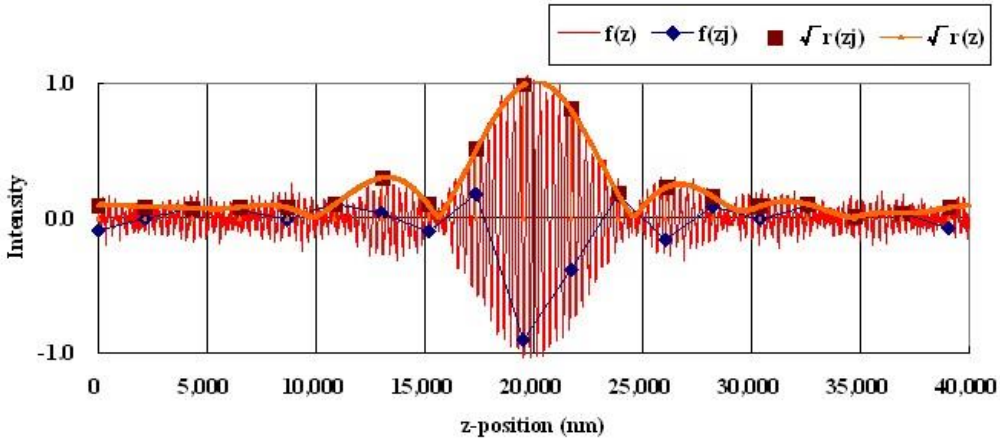

Fig. 2-9 Original interferogram $f(z)$, its sampled data $f(z_j)$ and the reconstructed envelope function $\sqrt{r}(z)$ (with Gaussian noise added)

2.5 Actual sample experiments

Figure 2-10 shows the appearance of the profiler SP-500, which is a product incorporating the above algorithm, and Fig. 2-11 shows the configuration. Figure 2-12 shows the results of measuring a standard step (nominal value 9.95 μm) at a measurement speed of 25.5 μm/s (sampling interval 0.85 μm) using this device. The sampling interval is about 6 times the Nyquist interval, but almost accurate surface shape is measured.

The average value of the step was 10.03 μm, the repeatability (σ; pixel-pixel) was about 0.1 μm, and the measurement time of 128x120 pixels was 0.8 s. An example of the sampled intensity data, reconstructed waveform, and envelope function is shown in Fig. 2-13.

In addition, Fig. 2-14 shows the results of measuring IC bumps with a height of about 40 μm at a measurement speed of 54 μm/s (sampling interval 1.8 μm). It can be seen that the measurement can be performed with practically sufficient accuracy.

Fig. 2-10 Surface profiler SP-500

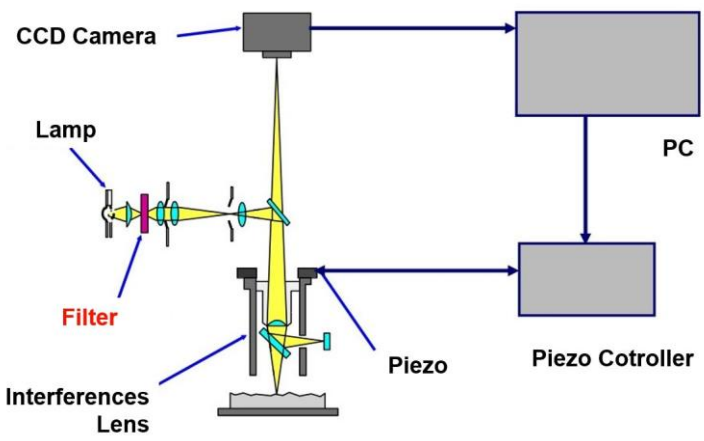

Fig. 2-11 Configuration of surface profiler SP-500

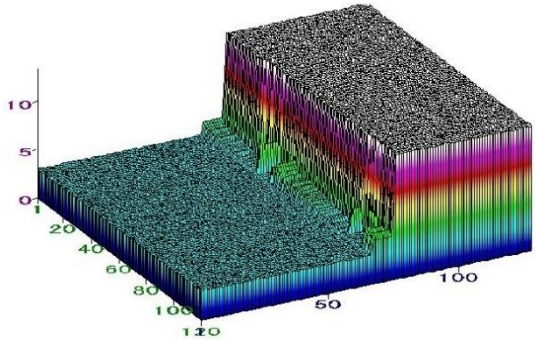

Fig. 2-12 Three dimensional profile of a step height measured by the SEST algorithm

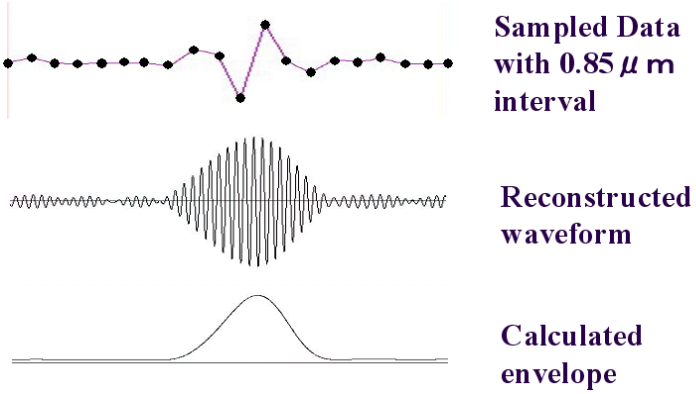

Fig. 2-13 Sampled data, reconstructed waveform and envelope

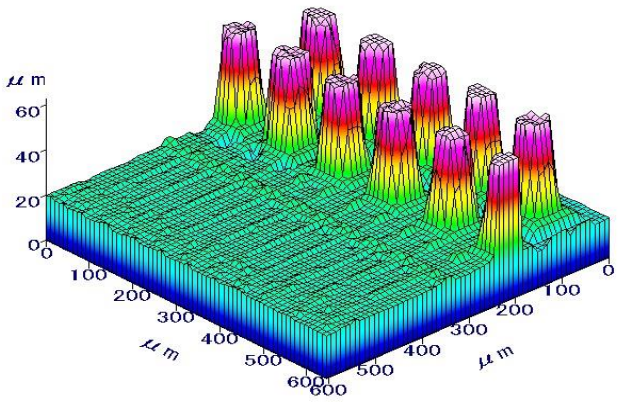

Fig. 2-14 Measurement of IC bumps using the SEST algorithm with 54 μm/s speed

2.6 Selection of shutter speed

Image blurring becomes a problem when the scanning speed is increased, so it is necessary to increase the shutter speed of the camera. A faster shutter speed is better, but there is a limit because the image becomes dark. The results of investigating the effect of the shutter speed on the measured height are shown in Fig. 2-15. The measurement target is a standard step (nominal value 9.947 μm), and the scanning speed is 50.4 μm/s. A shutter speed of about 1/1000s is optimal.

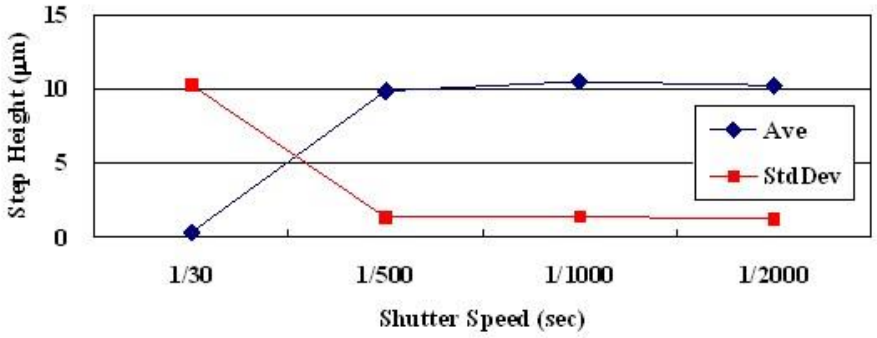

Fig. 2-15 Effect of camera shutter speed

2.7 Scanning speed and repeatability

The step standard of about 10 μm was repeatedly measured by changing the scanning speed (= sampling interval), and the average value of the step and the repeatability (σ) were obtained. The results are shown in Fig. 2-16. Theoretically, signal reconstruction is possible if the interval is equal to or less than the interval upper limit of Eq. (2-20), but in reality, the sampling points are finite and noise is added, so the wider the sampling interval, the more the measurement accuracy is reduced.

Looking at the results, we can see that there is a periodic optimal sampling interval. This interval is considered to correspond to the allowable range shown in Fig. 2-3, and the center of each range can be expressed by the following equation when $\lambda_c >> \lambda_b$.

$$\Delta = (I + 1/2)(\lambda / 4), \qquad (2\text{–}21)$$

where I is an integer. When λ is 600 nm, Δ becomes 150(I+1/2), which is similar to the result in Fig. 2-16. Practically, the scanning speed is selected from this optimum sampling interval (shown as minimum values in Fig. 2-16).

From the experimental results, it can be seen that submicron measurement repeatability can be obtained even at a scanning speed of 60 μm/s (sampling interval=2.0 μm; equivalent to about 13 times the Nyquist interval). This data shows the repeatability for each pixel, and in usual height or step measurements, the repeatability can be further improved by averaging the data of multiple pixels.

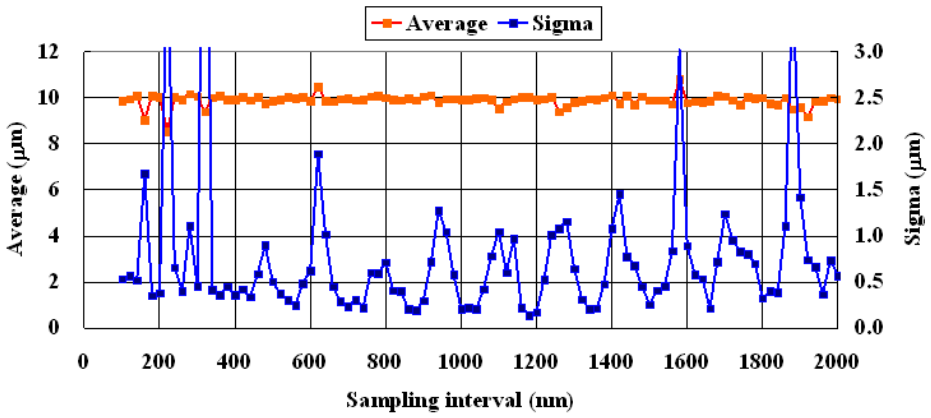

Fig. 2-16 Average height and repeatability (pixel-to-pixel) vs sampling interval of SEST method

The repeatability data described above is based on the SEST method, but when the scanning speed is low, the conventional low-pass filter method is superior. Therefore, in actual operation, the algorithm used is switched according to the scanning speed, the low-pass filter method is used at low speeds, and the SEST method is used at high speeds. As a result, the relationship between scanning speed and repeatability is as shown in Fig. 2-17. Since there is a trade-off between accuracy and measurement time, select the optimum speed according to the intended use.

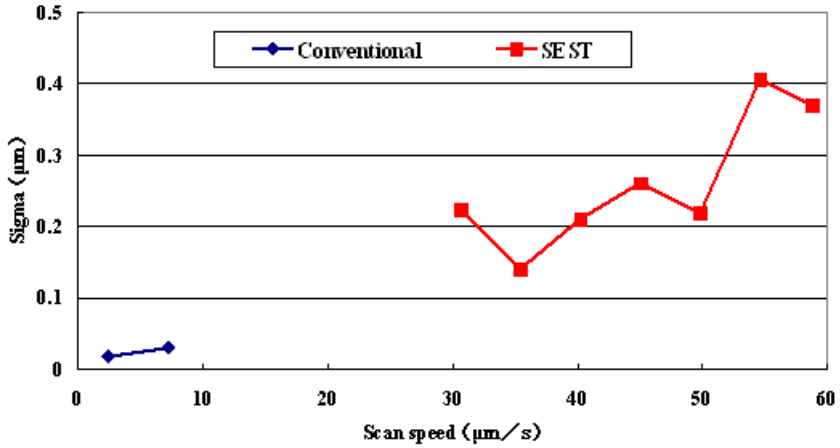

Fig. 2-17 Repeatability (pixel-to-pixel) vs scan speed in VSI method

2.8 Summary

In order to measure the surface profile using white light interference at high speed, we devised a new algorithm to find the peak position from the interference waveform. Applying the bandpass sampling theorem, the envelope function of the interference waveform is directly reconstructed from the sub-Nyquist sampling data. As a result, the sampling interval can be increased to about 10 times that of the conventional method, achieving the world's fastest scanning speed of 60 μm/s). [2] We have developed and commercialized a profiler incorporating this algorithm and confirmed its practicality.

This is an English translation of the article:
Katsuichi Kitagawa, "Chapter 2: High-speed white light interferometry",
in "Study on industrial surface profile measurement method based on optical interferometry", pp. 14-26, Doctoral Dissertation, University of Tokyo (2011)
(original in Japanese; translated by the author in Aug. 2020)

[2] Since then, the speed of the camera has increased, and a scanning speed of 214 μm/s has been achieved using a 7x camera (210 fps). This is the highest speed in the industry today. Note that the speed of the piezo actuator is rate-limiting (bottleneck).